Near-field imaging of quantum cascade laser transverse modes

Nanfang Yu[1], Laurent Diehl[1], Ertugrul Cubukcu[1], Christian Pflügl[1], David Bour[2, a], Scott Corzine[2, b], Jintian Zhu[2], Gloria Höfler[2, c], Kenneth B. Crozier[1], and Federico Capasso[1]*

[1]*School of Engineering and Applied Sciences, Harvard University Cambridge, Massachusetts 02138, USA*
[2]*Agilent Laboratories, 3500 Deer Creek Road, Palo Alto, California 94304, USA*
Current affiliations:
[a]*Bridgelux Inc, 1225 Bordeaux Dr, Sunnyvale, California 94089, USA*
[b]*Infinera HQ, 169 Java Dr, Sunnyvale, California 94089, USA*
[c]*Argos Tech LLC, 3671 Enochs St, Santa Clara, California 95051, USA*
**Corresponding author: capasso@seas.harvard.edu*

Abstract: We report near field imaging of the transverse lasing modes of quantum cascade lasers. A mid-infrared apertureless near-field scanning optical microscope was used to characterize the modes on the laser facet. A very stable mode pattern corresponding to a TM_{00} mode was observed as function of increasing driving current for a narrow active region quantum cascade laser. Higher order modes were observed for devices with a larger active region width-to-wavelength ratio operated in pulsed mode close to threshold. A theoretical model is proposed to explain why specific transverse modes are preferred close to threshold. The model is in good agreement with the experimental results.

OCIS codes: (140.5965) Semiconductor lasers, quantum cascade; (030.4070) Modes; (180.4243) Near-field microscopy; (250.5403) Plasmonics.

References and links

1. A. E. Siegman, "Defining, measuring, and optimizing laser beam quality," in *Proceedings of SPIE. Vol. 1868: Laser Resonators and Coherent Optics: Modeling, Technology, and Applications*, A. Bhowmik, ed. (the International Society for Optical Engineering, 1993), pp. 2-12.
2. E. Betzig and J. K. Trautmann, "Near-field optics: microscopy, spectroscopy, and surface modification beyond the diffraction limit," Science **257**, 189-195 (1992).
3. S. K. Buratto, J. W. P. Hsu, J. K. Trautman, E. Betzig, R. B. Bylsma, C. C. Bahr, and M. J. Cardillo, "Imaging InGaAsP quantum-well lasers using near-field scanning optical microscopy," J. Appl. Phys. **76**, 7720-7725 (1994).
4. U. Ben-Ami, N. Tessler, N. Ben-Ami, R. Nagar, G. Fish, K. Lieberman, G. Eisenstein, A. Lewis, J. M. Nielsen, and A. Møeller-Larsen, "Near-infrared contact mode collection near-field optical and normal force microscopy of modulated multiple quantum well lasers," Appl. Phys. Lett. **68**, 2337-2339 (1996).
5. F. Zenhausern, M. P. O'Boyle, and H. K. Wickramasinghe, "Apertureless near-field optical microscope," Appl. Phys. Lett. **65**, 1623-1625 (1994).
6. A. Lahrech, R. Bachelot, P. Gleyzes, and A. C. Boccara, "Infrared-reflection-mode near-field microscopy using an apertureless probe with a resolution of λ/600," Opt. Lett. **21**, 1315-1317 (1996).
7. G. Wurtz, R. Bachelot, and P. Royer, "Imaging a GaAlAs laser diode in operation using apertureless scanning near-field optical microscopy," Eur. Phys. J. AP. **5**, 269-275 (1999).
8. V. Moreau, M. Bahriz, R. Colombelli, P. Lemoine, Y. D. Wilde, L. R. Wilson, and A. B. Krysa, "Direct imaging of a laser mode via midinfrared near-field microscopy," App. Phys. Lett. **90**, 201114 (2007).
9. B. Knoll and F. Keilmann, "Enhanced dielectric contrast in scattering-type scanning near-field optical microscopy," Opt. Commun. **182**, 321-328 (2000).
10. T. Taubner, R. Hillenbrand, and F. Keilmann, "Nanoscale polymer recognition by spectral signature in scattering infrared near-field microscopy," Appl. Phys. Lett. **85**, 5064-5066 (2004).
11. M. Brehm, T. Taubner, R. Hillenbrand, and F. Keilmann, "Infrared spectroscopic mapping of single nanoparticles and viruses at nanoscale resolution," Nano Lett. **6**, 1307-1310 (2006).
12. L. Diehl, D. Bour, S. Corzine, J. Zhu, G. Höfler, M. Lončar, M. Troccoli, and F. Capasso, "High-temperature continuous wave operation of strain-balanced quantum cascade lasers grown by metal organic

#86281 - $15.00 USD Received 9 Aug 2007; revised 21 Sep 2007; accepted 21 Sep 2007; published 27 Sep 2007

vapor-phase epitaxy," Appl. Phys. Lett. **89**, 081101 (2006).
13. M. Troccoli, S. Corzine, D. Bour, J. Zhu, O. Assayag, L. Diehl, B. G. Lee, G. Höfler, and F. Capasso, "Room temperature continuous-wave operation of quantum-cascade lasers grown by metal organic vapour phase epitaxy," Electron. Lett. **41**, 1059-1060 (2005).
14. The complex refractive index of the active region is calculated by taking the weighted average of the complex refractive indexes of the two constituent materials (AlInAs and InGaAs). This is a good approximation because the wavelength in the laser material is significantly larger than the thickness of each individual material layer (typically 1~4 nm).
15. J. Guthrie, G. L. Tan, M. Ohkubo, T. Fukushima, Y. Ikegami, T. Ijichi, M. Irikawa, R. S. Mand, and J. M. Xu, "Beam instability in 980-nm power lasers: experiment and analysis," IEEE Photon. Technol. Lett. **6**, 1409-1411 (1994).
16. M. F. C. Schemmann, C. J. van der Poel, B. A. H. van Bakel, H. P. M. M. Ambrosius, A. Valster, J. A. M. van den Heijkant, and G. A. Acket, "Kink power in weakly index guided semiconductor lasers," Appl. Phys. Lett. **66**, 920-922 (1995).
17. G. L. Tan, R. S. Mand, and J. M. Xu, "Self-consistent modeling of beam instabilities in 980-nm fiber pump lasers," IEEE J. Quantum Electron. **33**, 1384-1395 (1997).
18. W. W. Bewley, J. R. Lindle, C. S. Kim, I. Vurgaftman, J. R. Meyer, A. J. Evans, J. S. Yu, S. Slivken, and M. Razeghi, "Beam steering in high-power CW quantum-cascade lasers," IEEE J. Quantum Electron. **41**, 833-841 (2005).

1. Introduction

Understanding how the transverse mode structure and more generally the beam quality (divergence, spatial coherence, etc.) [1] of a semiconductor laser varies as a function of pumping current or ridge width is crucial for applications that require coupling of the laser output into another optical element. Measuring the laser far-field angular distribution is commonly used for this purpose. Measuring its emission pattern in the near field is much more challenging as the latter extends only over a very short distance from the laser facet. In addition, the interesting mode features in the near field have a lateral dimension roughly equal to or smaller than the free space wavelength divided by the effective refractive index of the mode. Because of their low spatial resolution due to the diffraction limit, traditional optical methods cannot be used for near-field measurements.

The Near-field Scanning Optical Microscope (NSOM) was introduced to circumvent this problem [2]. In this technique, a tapered fiber with a subwavelength aperture at its end is scanned in the near field of the sample. The intensity of the light collected by the fiber is directly related to the sample's near field. This method has been used to image the transverse mode of λ=1.55 μm telecommunication lasers [3,4]. The above approach is not suitable in the mid-infrared (mid-ir) regime because of the difficulty of finding a good compromise between high spatial resolution, requiring a small aperture at the end of the tapered fiber, and a reasonable power throughput. The apertureless-NSOM (a-NSOM) is a solution to this problem [5,6]. In this technique, a sharp tip with nanometric apex curvature oscillates in the vicinity of the sample's surface and scatters light from the near field out in the far field where it is analyzed. A-NSOM has been used in the imaging of the transverse mode of a λ=780 nm laser diode [7]. Recently, an a-NSOM was also used to image the evanescent field of the Fabry-P**é**rot standing waves on the so-called "air-waveguide" of a mid-ir quantum cascade laser (QCL) [8].

In this work, we present the results obtained by scanning the tip of an a-NSOM on the output facet of buried heterostructure (BH) QCLs with wavelengths of 5.3 μm and 7.0 μm that are operated in pulsed mode at room temperature. The near-field images acquired show clearly that for very narrow devices, only the TM_{00} mode is present and that for devices with broader ridge, high order modes are preferred at a driving current close to the laser threshold.

2. Experimental setup

A schematic drawing of the experimental setup is shown in Fig. 1. The a-NSOM is based on a commercial atomic force microscope (AFM) (PSIA XE-120) operating in tapping mode. In a measurement, an AFM tip oscillates at a frequency close to its resonant frequency f_o (typically between 40 kHz and 80 kHz) and during each oscillation, the tip makes contact with the sample, allowing a near field and a topography image to be simultaneously obtained. The

#86281 - $15.00 USD Received 9 Aug 2007; revised 21 Sep 2007; accepted 21 Sep 2007; published 27 Sep 2007

maximum amplitude of the oscillation is about 40 nm. The AFM tips used are coated with gold (40 nm thick) and are electrically insulated from the tip mount so that the current flowing through the QCL active region is not altered while the tip is in contact with the facet. Electrical shorting of the QCL by the AFM tip is negligible because the tip radius of curvature, typically 15 nm, is smaller than the thickness of one stage of the devices used (52 nm for the λ=5.3 μm QCLs and 44 nm for the λ=7.0 μm QCLs). There are 30 stages in each device.

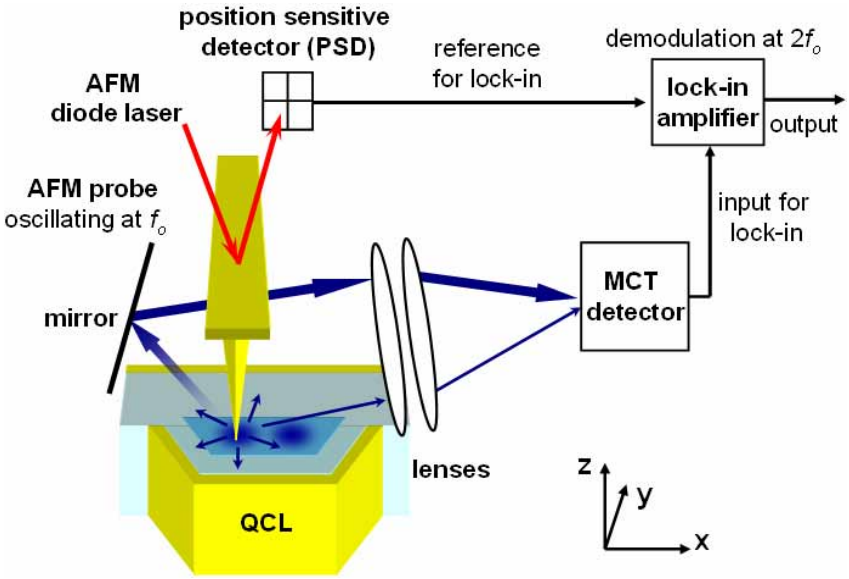

Fig. 1. A sketch of the apertureless mid-ir near-field scanning optical microscope used to characterize transverse modes on the facet of quantum cascade lasers (QCLs). The detector records the interference signal between the radiation directly scattered into the far field by the apex of the AFM tip and the laser reflected from the mirror. Demodulation is performed at the second harmonic of the tapping frequency of the AFM tip in order to sufficiently suppress the contributions from the background light. Note that QCLs are TM polarized, i.e. the polarization of electric field is along y direction denoted in the figure. Thus the scattered near field would occur preferentially in the direction perpendicular to y. This is because the electric dipoles induced by the laser emission inside the AFM tip and the QCL material are polarized in the y direction. These dipoles radiate preferentially on the plane that is perpendicular to their axes. Accordingly, the lenses and detectors are placed along the x direction to maximize collection efficiency.

As shown in Fig. 1, the near field scattered by the AFM tip was collected and focused onto a liquid-nitrogen-cooled mercury cadmium telluride (MCT) detector by two f/1.5 ZnSe lenses. The near field scattered into the far field is very weak due to the tiny area of the tip apex. In order to enhance the near-field detection sensitivity, instead of recording the intensity of the scattered near field directly, the interference between the scattered near field and an intense reference field is detected. This is realized by placing a small mirror with an appropriate orientation near the front or the back facet of the QCL to reflect directly the laser output to the collecting lenses. At the detector, the interference term containing the product of the radiation scattered into the far field by the apex of the AFM tip and the reflected laser is measured. The latter is a constant or a slow-varying function of the position of the tip as it scans the facet, so the NSOM image is a map of the amplitude of the near field [9]. The intensity of the scattered near field is also detected but it is much weaker than the interference term and contributes little to the NSOM images. The main difference between our detection method and the interferometric technique in Refs. [9-11] where an oscillating mirror is employed is that in our experiments the mirror is kept fixed because of space constrains. In our case, therefore, there

#86281 - $15.00 USD Received 9 Aug 2007; revised 21 Sep 2007; accepted 21 Sep 2007; published 27 Sep 2007

is no detection of the phase of the near field but just enhancement of the detection sensitivity. The interference scheme of Fig. 1 is particularly useful in imaging of the laser modes near threshold due to limited power output.

The detected signal was fed into a lock-in amplifier. In order to discriminate efficiently between contributions from the scattered near field and the field scattered from the shaft or the cantilever of the AFM tip, the lock-in amplifier needs to be set to demodulate at a harmonic nf_o of the AFM tip oscillating frequency f_o [9]. The reason for this is well understood based on a model in which the scattering cross section C_{scat} of a coupled system composed of a polarizable sphere and a plane sample in the vicinity is shown to be highly nonlinear with respect to their separation [9]. We used $2f_o$ for all the measurements.

3. Near-field imaging of a narrow active region quantum cascade laser

We first investigated the near field of a BH QCL emitting at λ=5.3 μm with an active region width of approximately 3 μm. A scanning electron microscope (SEM) image of the laser facet is shown in Fig. 2(a). The structure, processing, and the performance of similar devices are described in references 12 and 13. Figs. 2(c)-2(e) show $2f_o$ NSOM mode images of the device at different driving currents. Small markers, visible on the SEM image, were drilled at the corners of the cross section of the trapezoidal active region [labeled as 1 in Fig. 2(a)] by focused ion beam (FIB) milling, allowing the NSOM mode images to be correlated with the location of the active region.

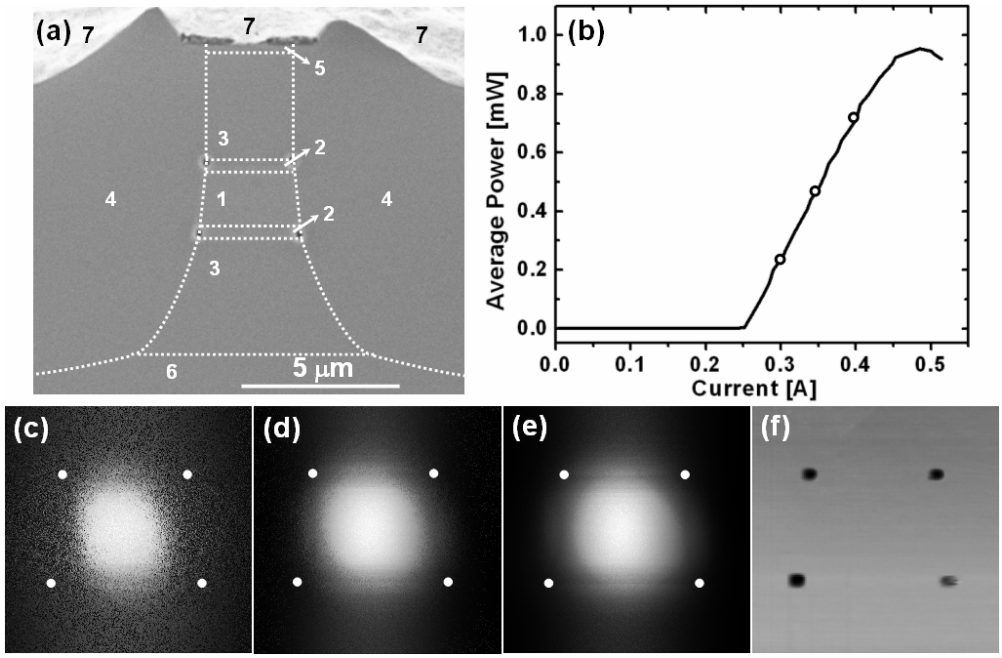

Fig 2. (a). Scanning electron microscope image of the facet of a λ=5.3μm quantum cascade laser (QCL) with an active region width ≈3 μm. The numbers in the image indicate: 1 active region, 2 InGaAs cladding layer, 3 InP cladding layer, 4 InP regrown region, 5 InP plasmon layer, 6 InP substrate, 7 gold top contact. (b) Measured light output vs. current (LI) curve of the QCL. The open circles on the curve indicate the working conditions under which images (c), (d), and (e) were taken. The LI curve was taken at room temperature in pulsed mode. (c), (d), and (e) Near-field $2f_o$ images of the laser mode for a driving current of 300, 350, and 400 mA, respectively. The white dots in each near field image indicate the corners of the area comprising the active region and the InGaAs cladding layers. (f) The AFM topography taken simultaneously with (c). The size of the images (c)-(f): 5.3 μm×5.3 μm.

#86281 - $15.00 USD Received 9 Aug 2007; revised 21 Sep 2007; accepted 21 Sep 2007; published 27 Sep 2007

The three NSOM mode images shown in Figs. 2(c)-2(e) were measured with the device operating in pulsed mode at three different driving currents corresponding to the three open circles on the light output vs. current curve presented in Fig. 2(b). The fact that the laser was operated in pulsed mode does not play a role in the optical measurements, because the repetition rate (500~800 kHz, current pulse width 125 ns for all measurements) was significantly higher than the tapping frequency of the AFM tip. The near field images Figs. 2(c)-2(e) exhibit clearly a single lobe located at the center of the active region. Two-dimensional mode calculations performed with the commercial software COMSOL Multiphysics 3.3 show indeed that only the fundamental mode TM_{00} is supported by the narrow waveguide core of the laser tested. Note that experimentally, the magnitude of the NSOM signal, demodulated at $2f_o$, showed an exponential increase as the tip approached the laser facet, confirming that the signal detected is from the near field. In order to further verify that the features observed in our near-field data are not artifacts, we compared various measurements obtained with the same device under the same electrical conditions, but in different experimental configurations. For example, we used different types of AFM tips and in addition rotated the QCL investigated in the horizontal plane thus using a different angle between the orientation of the cantilever of the AFM tip and the QCL growth direction. The power of the collected signal was different in each case due to different collection efficiencies but the laser mode profiles were identical, demonstrating our ability to measure correctly the near-field of our samples.

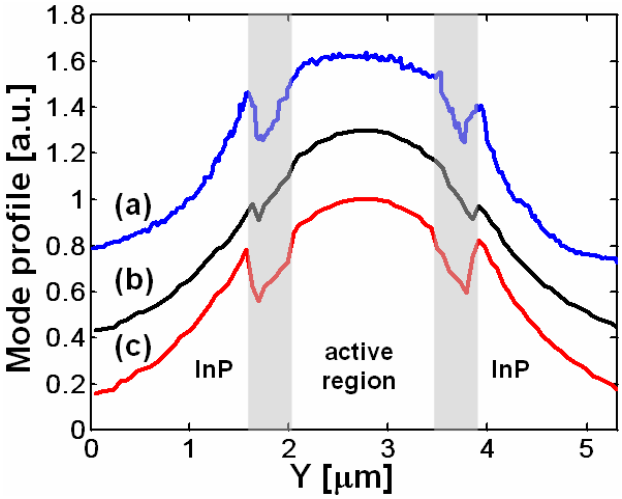

Fig. 3. (a). Line scan of the mode profile normal to the quantum cascade laser layers of the λ=5.3μm device with a 3 μm wide active region. The scan is taken vertically along the center of Fig. 2(e) and is the average of ten traces. (b) Mode profile calculated using the COMSOL software. (c) Mode profile in (b) corrected for the effect of different scattering cross sections associated with the distribution of complex refractive indexes on the laser facet. The shaded regions correspond to two thin InGaAs cladding layers; between them is the active region and outside of them are the InP cladding layers. The three curves are shifted vertically for clarity.

#86281 - $15.00 USD Received 9 Aug 2007; revised 21 Sep 2007; accepted 21 Sep 2007; published 27 Sep 2007

More interesting features can be observed in the mode images shown in Fig. 2. Curve (a) in Fig. 3 shows a line scan vertically across Fig. 2(e). Two dips are clearly visible on the curve, which corresponds to the two horizontal dark bands across Fig. 2(e). They correspond to the two thin InGaAs cladding layers adjacent to the active region. Similar dark bands can be identified in the other mode images in Fig. 2 and Fig. 4. There are two contributions to these dips in the line scan or the dark bands in the mode images. One is the non-monotonic change of the mode intensity in these regions due to the non-monotonic change in the refractive index while going from the active region to the InP cladding layers. A vertical line scan of the calculated electric field magnitude distribution of the mode only considering this contribution is shown as curve (b) in Fig. 3. Apparently, it is not able to account for the relatively deep dips in the line scan of the near field image. The other contribution is related to the spatial variation of the complex refractive index of the laser facet. According to the model proposed in reference 9, the scattering cross section C_{scat} of a probe-sample coupled system, namely, an AFM tip oscillating on a plane sample, is a function of the complex refractive index of the sample material. This model has been used in high-resolution mid-infrared near-field microscopy, for instance, of polymers and viruses [10, 11]. We calculated the second harmonic component of the temporally modulated C_{scat} for an AFM tip oscillating on the different regions of the laser facet. For a λ=5.3 μm QCL, the complex refractive indexes of the active region [14], the InGaAs cladding layer, and the InP cladding layer that constitute the laser waveguide vertically are $3.2773+i1.76\times10^{-4}$, $3.3710+i0.77\times10^{-4}$, and $3.0754+i1.44\times10^{-4}$, respectively (see Fig. 2(a) for the location of these regions). The ratios of the second harmonic components are 1.00/0.91/1.22 for these three regions. Here, the AFM tip is modeled as a polarizable sphere with a radius of 20 nm and is assumed to be oscillating perpendicular to the laser facet with an amplitude of 30 nm, which is similar to our experimental conditions in which the tip is tapping nearly vertically on the laser facet. The mode profile calculated with the correction from these ratios is shown as curve (c) in Fig. 3, which is in good agreement with the line scan of the mode image [curve (a)]. The aforementioned ratios of the second harmonic components are 1.00/0.94/1.27 for a λ=7.0 μm QCL, very similar to these of the λ=5.3 μm QCL. It is estimated from the line scan of the mode profile that the resolution of the setup is about 120 nm, which corresponds to $\lambda/40$.

#86281 - $15.00 USD Received 9 Aug 2007; revised 21 Sep 2007; accepted 21 Sep 2007; published 27 Sep 2007

4. Near-field imaging of broad active region quantum cascade lasers

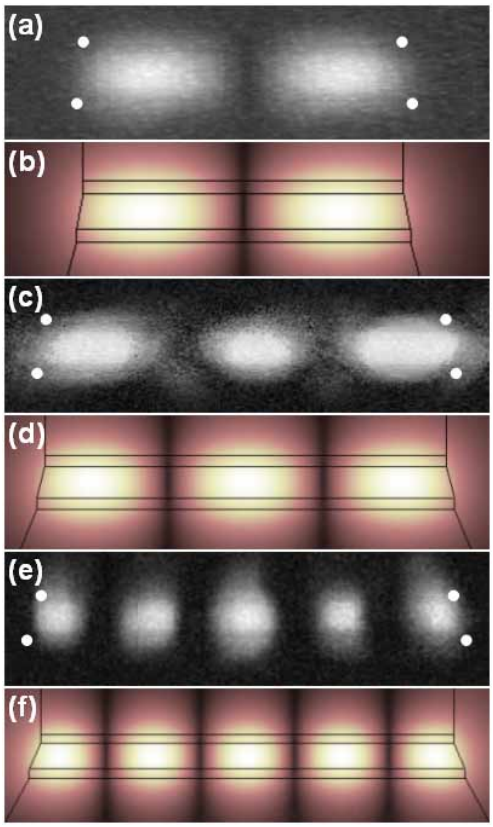

Fig. 4. Near field mode profile of three λ=7.0 μm quantum cascade lasers (QCLs) with wide active regions. (a) and (b) NSOM image and simulation of the TM_{01} mode of a QCL with a 12 μm wide active region. Image size: 18 μm×5.0 μm. (c) and (d) NSOM image and simulation of the TM_{02} mode of a QCL with a 17 μm wide active region. Image size: 20 μm×5.6 μm. (e) and (f) NSOM image and simulation of the TM_{04} mode of a QCL with a 22 μm wide active region. Image size: 25 μm×6.9 μm. Simulation results shown are the distribution of the magnitude of the electric field, which is polarized essentially perpendicular to the layers of the QCL material. The black lines in each simulated mode image indicate the edges of different regions. White dots in each NSOM image indicate the corners of the area comprising the active region and the InGaAs cladding layers.

Additional near-field images were taken for three λ=7.0 μm BH QCLs with active region width 12 μm, 17 μm, and 22 μm, respectively, driven in pulsed mode just above the threshold current with an average output power on the order of 0.1 mW. The laser ridge length is 2.0 mm. The measurements obtained at room temperature are presented in Fig. 4, along with the results of COMSOL mode simulations. Again the dark bands are observed in the mode images Figs. 4(a), 4(c), and 4(e), which correspond to the InGaAs cladding layers. By comparing the near-field images and the calculations, it can be seen that the TM_{01} mode, the TM_{02} mode, and the TM_{04} mode are the preferred optical modes for the 12 μm, 17 μm, and 22 μm wide lasers, respectively.

The fact that the laser emission just above threshold is dominated by these specific transverse modes can be understood as follows. The transverse mode that has the smallest threshold current will be preferred. The latter is proportional to the figure of merit L defined by $L=(\alpha_w+\alpha_m)/\Gamma$, where α_w is the waveguide loss, α_m is the mirror loss, and Γ is the mode confinement factor. Γ and α_w can be obtained once the real and imaginary part of the

#86281 - $15.00 USD Received 9 Aug 2007; revised 21 Sep 2007; accepted 21 Sep 2007; published 27 Sep 2007

refractive index of each material composing the waveguide are known. The mirror losses α_m can be calculated using a simple two-dimensional ray optics model, allowing the angle φ between the propagation vector and the output facet of the laser to be determined and the Fresnel equations to deduce the value of the mirror reflectivity given the value of φ. Note that the Fresnel equations are a good approximation in our situation since the active region in the transverse direction is much wider (>5 times) than the wavelength in the laser active region (7 μm/3.3≈2 μm). As shown in Table 1, the quantities Γ and α_w remain essentially constant until the mode order increases up to a specific value satisfying an empirical formula: mode order × wavelength in the laser waveguide ≈ active region width/2. For transverse mode with mode order equal or larger than this value, the optical mode strongly leaks into the surrounding InP and a substantial part of the mode is in contact with the gold contacts, which results in a decrease of Γ and an increase of α_w. Table 1 also shows that the quantity α_m decreases monotonically as the mode order increases. This can be understood from the ray optics model described above: higher order modes impinge on the facet at a larger incidence angle compared to lower order modes, resulting in lower mirror loss $\alpha_m \propto \ln(1/R_1R_2)$, where R_1 and R_2 are the power reflectivities for the two laser facets, respectively. The values of the figure of merit L calculated for the various lateral modes supported by the 12, 17, and 22 μm wide devices are also given in Table 1. The results show that the transverse modes with the smallest value for L (in bold letters in Table 1) are the ones that are observed close to threshold, as displayed in Fig. 4. The conclusions of our calculations are thus in good agreement with the experiment.

Table 1. Calculations of the Mode Confinement factor, the Waveguide Loss, the Mirror Loss, and the Figure of Merit of Different Transverse Modes

Active Region Width [μm]	Transverse Mode	Mode Confinement Factor Γ	Waveguide Loss α_w [cm^{-1}]	Mirror Loss α_m [cm^{-1}]	Figure of Merit $(\alpha_m+\alpha_w)/\Gamma$ [cm^{-1}]
12	TM_{00}	0.517	6.758	6.080	24.85
	TM_{01}	**0.496**	**6.768**	**5.448**	**24.62**
	TM_{02}	0.447	7.107	4.199	25.27
17	TM_{00}	0.520	6.761	6.171	24.85
	TM_{01}	0.513	6.779	5.843	24.63
	TM_{02}	**0.497**	**6.856**	**5.250**	**24.35**
	TM_{03}	0.466	7.271	4.285	24.78
	TM_{04}	0.341	13.87	2.574	48.29
22	TM_{00}	0.522	6.759	6.210	24.87
	TM_{01}	0.518	6.764	6.009	24.67
	TM_{02}	0.511	6.773	5.656	24.34
	TM_{03}	0.499	6.804	5.121	23.91
	TM_{04}	**0.478**	**6.945**	**4.335**	**23.60**
	TM_{05}	0.420	8.557	3.118	27.82

The measured near field profiles showed single transverse mode profile only close to threshold. This was no longer the case when the current was increased from the threshold sometimes even by a small amount. Asymmetric near field mode profiles were observed that cannot be simply assigned to that of a single transverse mode. This indicates that additional transverse modes start to lase. Effects such as beam steering were also observed in the far field of some of the devices measured. It can be explained by a coherent superposition of the

#86281 - $15.00 USD Received 9 Aug 2007; revised 21 Sep 2007; accepted 21 Sep 2007; published 27 Sep 2007

various transverse modes supported by the waveguide when they lase simultaneously; evidence for this phenomenon has already been reported in the far field of diode lasers and high power QCLs [15-18]. A detailed analysis of the near- and far-field pattern of BH QCLs as a function of an increasing current will be discussed in a forthcoming publication.

5. Conclusions

The transverse modes of several buried heterostructure QCLs with various ridge width were characterized by a mid-ir a-NSOM. The near field images obtained for a λ=5.3 μm QCL with very narrow active region showed a very stable emission pattern corresponding to the fundamental mode TM_{00} up to high value of the injected current. Other measurements performed with wide ridge QCLs show lasing on a single high order transverse mode close to threshold. In each case, the mode profile was in good agreement with simulations. For the widest device, the TM_{04} mode was observed. By demodulating the detected signal at the second harmonic of the AFM tip oscillation frequency, the near-field imaging technique is able to reflect the material contrast inherent in the near-field images.

Acknowledgments

The authors acknowledge support from the Air Force Office of Scientific Research (AFOSR MURI on Plasmonics) and the Harvard Nanoscale Science and Engineering Center (NSEC). K. C. acknowledges support from NSEC, Draper Laboratory and DARPA. Support from the Center for Nanoscale Systems (CNS) at Harvard University is also gratefully acknowledged. Harvard-CNS is a member of the National Nanotechnology Infrastructure Network (NNIN).

#86281 - $15.00 USD Received 9 Aug 2007; revised 21 Sep 2007; accepted 21 Sep 2007; published 27 Sep 2007